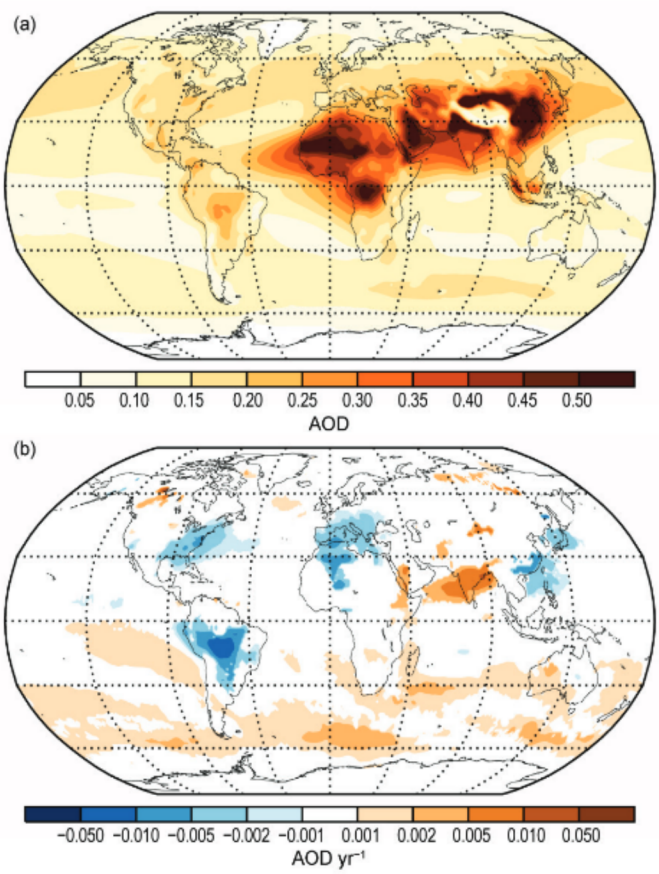

Fig. 2.44. (a) Total 550-nm AOD averages for 2003–14. (b) Linear trends from 2003 through 2015 of total AOD (AOD unit per year). Only trends that are statistically significant at the 95% level of confidence are shown.

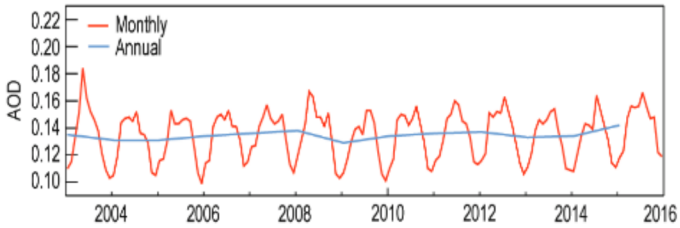

Fig. 2.45. Global averages of total AOD at 550 nm averaged over monthly (red) and annual (blue) periods for 2003–15.

basin, equatorial Africa, and Indonesia are caused by seasonal biomass burning. The linear trends highlight long-term decreases in anthropogenic aerosols over the eastern United States, Europe, and parts of southern China, while increases occurred over most of the Indian subcontinent. The area of decreasing trends in the southern Amazon basin is associated with reduced deforestation there (Chen et al. 2013). The decreasing trends over the northern Sahara and western Mediterranean indicate lower frequencies or intensities of dust episodes in these regions. Though many positive trends over the Southern Hemisphere oceans are not statistically significant, those that are could be an artefact of the MODIS Collection 5 observations used in the reanalysis. Time series of globally-averaged total AOD during 2003–15 (Fig. 2.45) show strong seasonality, typically with yearly maxima in March–April and August–September driven mainly by dust episodes and biomass burning in Africa and South America.

Aerosol monitoring relies on a multistream global observing system. Routine aerosol observations are mainly provided by two federated, ground-based networks: AERONET and Global Atmospheric Watch (GAW), which in 2015 operated 311 and >220 stations, respectively. MODIS satellite instruments on *Aqua* and *Terra* have continued to provide retrievals of AOD during 2015, while the Visible Infrared Imaging Radiometer Suite (VIIRS) on *Suomi NPP* has provided aerosol data products since 2013. Geostationary satellites are also increasingly being used to measure aerosols. For instance, AOD derived from Meteosat Second Generation (MSG) observations over Europe and Africa is available from 2014 (Carrer et al. 2014). AOD observations are now routinely incorporated into atmospheric models using data assimilation algorithms (e.g., Zhang et al. 2008; Benedetti et al. 2009; Inness et al. 2015b) to combine them with short-term forecasts. Such observationally constrained models can be used to build a reanalysis of atmospheric composition. Reanalyses can, to a large extent, be considered a good proxy for observed conditions. They provide whole atmosphere coverage and the ability to provide variables not routinely observed, such as the AOD of different aerosol types (e.g., dust, sea salt, and carbonaceous). However, their limitations should be kept in mind. To accommodate limited computing resources, models usually simplify aerosol processes and may not take into account all of the aerosol species and/or their interaction. This means that the atmospheric composition reanalysis aerosol products usually do not capture all of the observed variability and complexity of aerosol fields. Assessing the relative weight of observations and model values in the data assimilation scheme of such systems is not trivial; this can also lead to uncertainties (Inness et al. 2013).

4) Stratospheric ozone—M. Weber, W. Steinbrecht, C. Roth, M. Coldewey-Egbers, D. Degenstein, Y. E. Fioletov, S. M. Frith, L. Froidevaux, J. de Laat, C. S. Long, D. Loyola, and J. D. Wild

Total ozone columns in 2015 were close to the 1998–2008 average for most of the globe, except in extended regions at high latitudes in both hemispheres,

where ozone columns were largely below average (Plate 2.1q). The strong negative anomalies at high Southern Hemisphere latitudes reflect the large Antarctic ozone hole observed in September–December, whose size reached maximum values that were near the all-time record high (see section 6h).

In Fig. 2.46 the total ozone annual means from different data sources are shown for 1970–2015 in various zonal bands: near-global (60°S–60°N), midlatitudes in both hemispheres (35°–60°), and the inner tropics (20°S–20°N). Also shown are the polar time series in March (Northern Hemisphere, 60°–90°N) and October (Southern Hemisphere, 60°–90°S), the months when polar ozone losses are largest in each hemisphere. Poleward of 60°S, a record low October mean was observed (Fig. 2.46e). Weaker-than-usual dynamical wave activity in the Southern Hemisphere winter diminished transport from the tropics, reducing ozone at Southern Hemisphere midlatitudes and in the collar region of the polar vortex, and permitting a very stable and cold polar vortex. The high vortex stability and low temperatures resulted in larger-than-usual polar ozone losses and a near-record ozone hole in terms of size and persistence. Ozone annual mean columns at mid- to polar latitudes (35°–90°) in each hemisphere are largely determined by winter/spring ozone levels. These vary considerably with changes in stratospheric meteorological conditions (e.g., Steinbrecht et al. 2011; Weber et al. 2011; Kuttippurath et al. 2015). The year-to-year variability seen in all ozone time series also reflects quasi-biennial oscillation (QBO)-related variations extending from the tropics into the extratropics (Randel and Wu 1996; Strahan et al. 2015).

It is clear that the Montreal Protocol and its Amendments have been successful in stopping the multidecadal decline in stratospheric ozone by the late 1990s (WMO 2011). However, at most latitudes, it has not yet been possible to determine a statistically significant increase in total column ozone or lower stratosphere ozone because the expected small increases are masked by large interannual variability (e.g., Chehade et al. 2014; Coldewey-Egbers et al. 2014; Frith et al. 2014; Kuttippurath et al. 2015; Nair

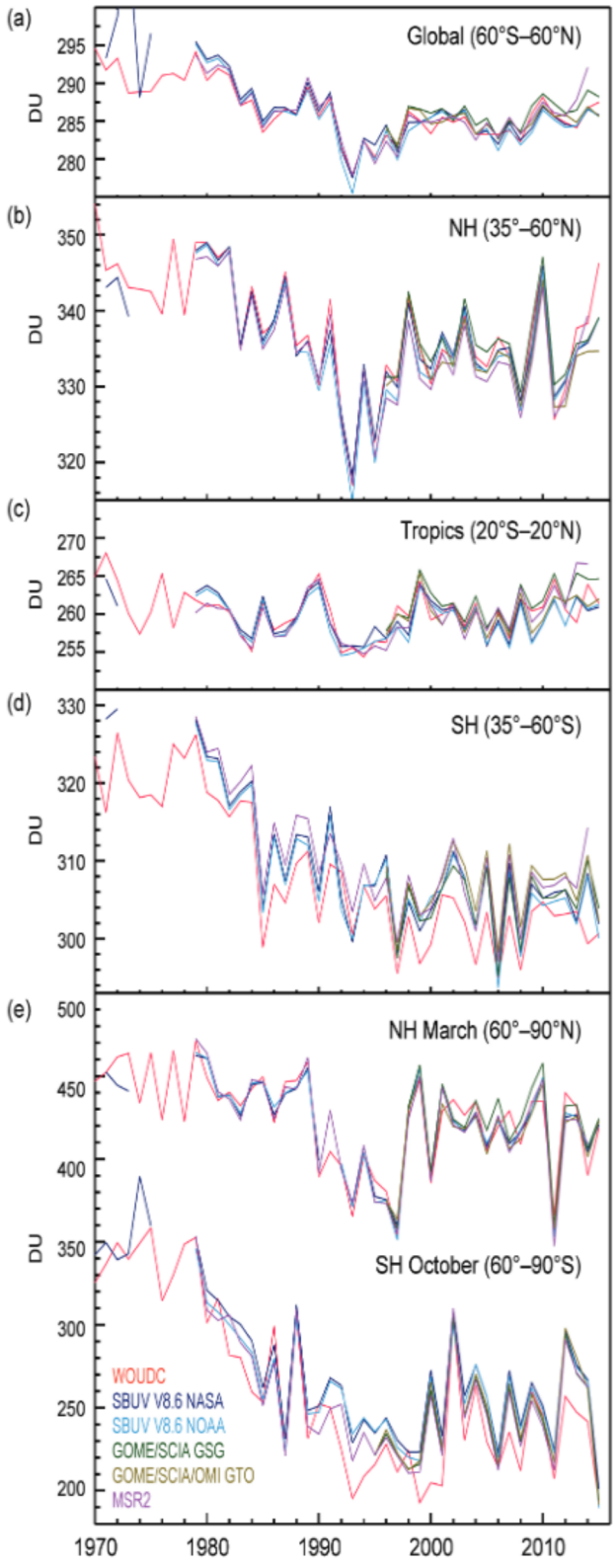

Fig. 2.46. Time series of annual mean total ozone in (a–d) four zonal bands and (e) polar (60°–90°) total ozone in Mar (Northern Hemisphere) and Oct (Southern Hemisphere). Data are from WOUDC ground-based measurements combining Brewer, Dobson, SAOZ, and filter spectrometer data (red: Fioletov et al. 2002, 2008); the BUV/SBUV/SBUV2 V8.6 merged products from NASA (MOD V8.6, dark blue, Chiou et al. 2014; Frith et al. 2014) and NOAA (light blue, Wild et al. 2012); the GOME/SCIAMACHY/GOME-2 products GSG from University of Bremen (dark green, Weber et al. 2011) and GTO from ESA/DLR (light green, Coldewey-Egbers et al. 2015); and the MSR V2 assimilated dataset extended with GOME-2 data (van der A et al. 2015). WOUDC values for 2015 are preliminary because not all ground station data were available in early 2016.

et al. 2015; de Laat et al. 2015). The 2015 total ozone columns in Fig. 2.46 are consistent with this overall picture and lie within the expected usual variations.

In the tropics, no discernible long-term trends in total column ozone have been observed for the entire 1970–2015 period (see Fig. 2.46). Ozone trends in the tropical lower stratosphere are mainly determined by tropical upwelling (related to changes in sea surface temperature). In a changing climate it is expected that tropical upwelling will increase and thus ozone will continue to decline (Zubov et al. 2013; WMO 2014). However, there is some evidence of a hiatus in tropical upwelling trends and corresponding lower stratospheric ozone trends during the last decade (Aschmann et al. 2014). Because tropospheric ozone contributes to the total ozone columns, trends in total ozone, despite major contributions from the lower stratosphere, may differ from trends in lower stratospheric ozone (Shepherd et al. 2014).

The most recent ozone assessment (WMO 2014) and studies (Nair et al. 2015; Harris et al. 2015) indicate that the clearest signs of significant ozone increases should occur in the upper stratosphere (2%–4% decade^{-1} at ~2 hPa or 40 km; see Fig. 2.47). However, there still are uncertainties associated with the various available data records and with the proper interpretation of statistical approaches used to derive and attribute trends (e.g., Nair et al. 2015; Kuttippurath et al. 2015; Harris et al. 2015). This is reflected in the updated Stratospheric Aerosol and Gas Experiment (SAGE)–Optical Spectrograph and Infrared Imager System (OSIRIS) record, which now better accounts for tangent altitude drifts, and in the updated Solar Backscatter Ultraviolet (SBUV) data from NOAA with improved inter-satellite adjustments. Overall, the 2015 annual means in Fig. 2.47 support the claim of recent increases in upper stratospheric, extra-polar ozone. These suggest the Montreal Protocol has successfully turned the previous downward trend in ozone into an ozone increase, at least in the upper stratosphere.

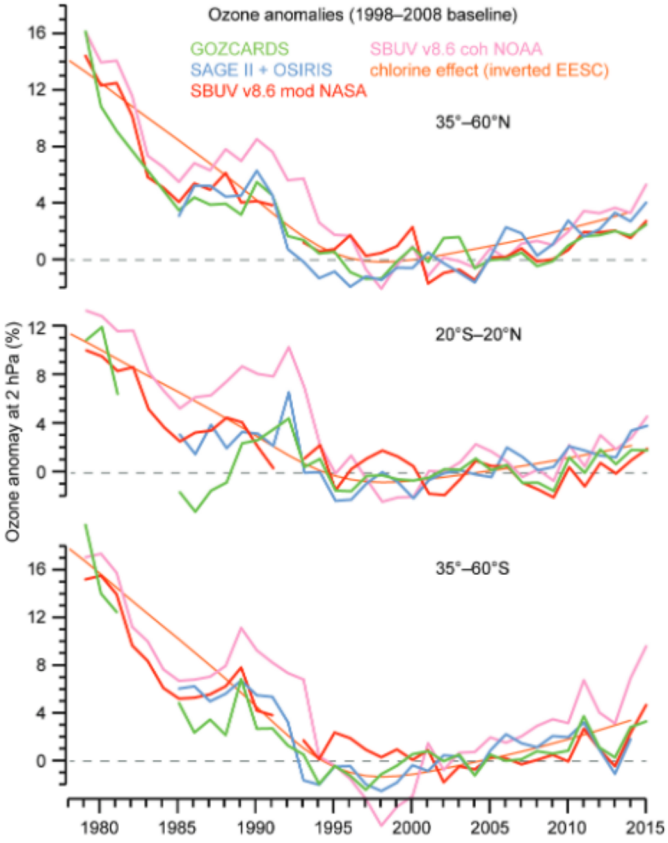

Fig. 2.47. Annual mean ozone anomalies at 2 hPa (~40 km, upper stratosphere) in three zonal bands. Data are from the merged SAGE II/OSIRIS (Bourassa et al. 2014) and GOZCARDS (Froidevaux et al. 2015) records and from the BUV/SBUV/SBUV2 v8.6 merged products from NASA (McPeters et al. 2013; Frith et al. 2014) and NOAA (Wild et al. 2012) (base period: 1998–2008). The orange curves represent EESC (effective equivalent stratospheric chlorine), scaled to reflect the expected ozone variation due to stratospheric halogens. Data points for 2015 are preliminary, because SAGE-OSIRIS data were not yet available after July 2015, and adjusted SBUV2 v8.0 data are used after July 2015 instead of v8.6 data, which are not available in early 2016.

5) Stratospheric water vapor—S. M. Davis, K. H. Rosenlof, D. F. Hurst, and H. B. Selkirk

Variations in stratospheric water vapor (SWV) over interannual-to-decadal timescales have the potential to affect stratospheric ozone (Dvortsov and Solomon 2001) and surface climate (Solomon et al. 2010). Throughout the first 10 months of 2015, water vapor mixing ratios in the tropical lowermost stratosphere were within 10% (0.4 ppm, μmol mol^{-1}) of the previous decade's average. Then, starting in November and continuing through December, tropical lowermost SWV increased to near-record levels, especially over the tropical western Pacific and Indian Ocean regions. The deep tropical-averaged (15°S–15°N) SWV anomaly at 82 hPa, based on data from the *Aura* Microwave Limb Sounder (MLS), was +0.7 ppm (+17%) in November and +0.9 ppm (+24%) in December. These values are in stark contrast to the weak negative (dry) tropical average anomalies of about −0.2 ppm (−6%) in November–December 2014 (Figs. 2.48, 2.49). Since the MLS record began in August 2004, the November–December 2015 anomalies at 82 hPa are surpassed only by +0.9 ppm (+25%) deep tropical anomalies in February–March 2011. The +0.7 ppm (+19%) average deep tropical anomaly at 100 hPa in November–December 2015 is the high-